Measurements of the stabilities of isolated retinal chromophores

L. Musbat, M. Nihamkin, and Y. Toker
Department of Physics and Institute of Nanotechnology, Bar-Ilan University, Ramat-Gan 5290002, Israel

J. M. Dilger
Spectrum Warfare Systems Department, NSWC Crane Division, Crane, Indiana 47522, USA

D. R. Fuller, T. J. El-Baba, and D. E. Clemmer
Department of Chemistry, Indiana University Bloomington, Indiana 47405, USA

S. Sarkar and L. Kronik
Department of Materials and Interfaces, Weizmann Institute of Science, Rehovot 7610001, Israel

A. Hirshfeld, N. Friedman, and M. Sheves
Department of Organic Chemistry, Weizmann Institute of Science, Rehovot 7610001, Israel
(Received 15 August 2016; published 19 January 2017)

The barrier energies for isomerization and fragmentation were measured for a series of retinal chromophore derivatives using a tandem ion mobility spectrometry approach. These measurements allow us to quantify the effect of charge delocalization on the rigidity of chromophores. We find that the role of the methyl group on the $C13$ position is pivotal regarding the ground state dynamics of the chromophore. Additionally, a correlation between quasi-equilibrium isomer distribution and fragmentation pathways is observed.

DOI: 10.1103/PhysRevE.95.012406

I. INTRODUCTION

One of the most basic aspects of a molecule is its structure. Even for small molecules structure is hard to determine as many stable isomers can be present simultaneously. In order to understand the electronic ground state dynamics, it is important to map the different isomers and understand their energetics (i.e., determine the relative energies and the barrier energies for isomerization). Until recently, this information could only be derived through quantum chemical calculations or deduced indirectly; however, recently Pierson *et al.* [1] introduced a novel experimental method to measure ground state energetics based on a tandem ion mobility spectrometry (IMS) mass spectrometry (MS). This technique, known as IMS-IMS-MS can be applied to any molecular ion. By comparing different derivatives of a given molecular ion, one can deduce how slight structural changes affect its rigidity and stability. Here we apply this technique to the important case of the retinal protonated Schiff base (RPSB).

The RPSB is a particularly interesting molecule as its proper function is imperative for sight. The primary event in animal vision is photoisomerization of the RPSB from the 11-*cis* configuration Fig. 1(a) to the *all-trans* structure Fig. 1(b) [2,3]. In bacteriorhodpsin proteins photoisomerizations occur from the *all-trans* isomer to the 13-*cis* structure [Fig. 1(c)]. Within Opsin proteins this photoisomerization is known to be specific, efficient (quantum efficiency of $>60\%$) [4], and ultrafast (occurs on a time scale of less than 200 fs) [5]. The barrier energy for this isomerization is critical for our understanding of vision as it determines the rate of 'dark counts', and has been found to inversely correlate with the absorption wavelength, a phenomenon known as the 'Barlow correlation' [6,7].

In arriving at a quantum mechanical understanding of the RPSB dynamics, gas phase experiments are instrumental as they can be directly compared with high level quantum calculations [8]. Indeed, gas phase measurements of the absorption of the RPSB have contributed to the understanding of the color tuning mechanism of the RPSB [9]. Tandem mass-spectrometry experiments (MS-MS) have shown that photofragmentation as well as low energy collision induced dissociation of the RPSB result in one prominent charged fragment which cannot be explained by any simple bond cleavage along the polyene chain of the chromophore, but does correspond to the emission of the central section of the molecule (between $C10$ and $C15$, indicated in red in Fig. 1(b) while tying together its both ends [10–12]. This occurs through a series of isomerizations and cyclizations, and the formation of the compact intermediate isomers shown in Fig. 1(d) and 1(e). Notably, this dynamics does not happen within the protein, as following the first isomerization—the energy is transferred to the surrounding protein—and lost from the chromophore.

Understanding the biologically important isomerizations of the RPSB as well as the intriguing cyclization dynamics make RPSB an ideal test case for IMS-IMS-MS measurements. Indeed Coughlan *et al.* have performed photoisomerization studies of the RPSB using IMS-IMS-MS and measured the difference in absorption cross section between different isomers [13,14]. They have also used IMS to propose a mechanism for the gas phase fragmentation of the RPSB [11] which we have later confirmed using isotope labeling mass spectrometry [12]. Using collision induced isomerization we have determined the barrier energies for isomerization of the RPSB and have shown that the barrier energy for the biologically important isomerization is much lower in the gas phase [15]. Thus, the protein has an important role in increasing the barrier energy and regulating the rate of dark counts.

 ©2017 American Physical Society

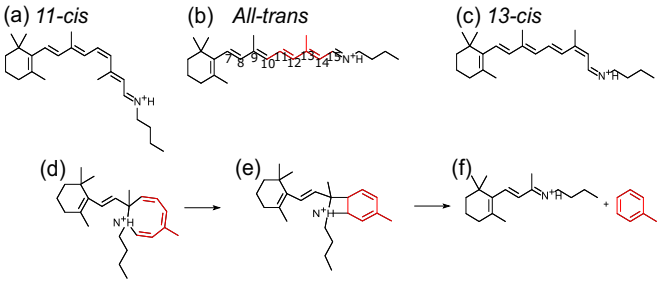

FIG. 1. Several of the important isomers of the RPSB. In animal vision the native state of the chromophore is the 11-*cis* isomer shown in (a), which photoisomerizes into the *all-trans* isomer (b). In bacteriorhodopsin the native state is the *all-trans* one and photoisomerization results in the 13-*cis* isomer (c). The gas phase fragmentation of the RPSB involves the formation of cyclized isomers (d) and (e), eventually resulting in Toluene emission (f).

In the present work we use IMS-IMS to measure the barrier energies of a series of retinal derivatives. We demonstrate that even small changes in the structure of the chromophore have a significant effect on its rigidity and stability. In particular, we compare a series of retinal derivatives in which the positive charge is less localized than in the RPSB and show that charge localization results in an increase in barrier energies for isomerizations. We also show that the methyl on the $C13$ position has a vital role in the ground state dynamics of the chromophore. Finally, we show a correspondence between the fragmentation mechanism of the chromophore with the distribution of isomers formed at high internal excitation energies. These findings may help explain the reason this chromophore is the sole photon detector used in every known form of animal vision.

II. IMS-IMS-MS OF RPSB

Experiments were conducted using the two-meter IMS-IMS-MS instrument which was described in detail previously [1,16]. Briefly, ions produced by nano-spray are accumulated before the entrance of the first drift tube and then pulsed into the drift tube at a rate of 10 Hz. Within the drift tube ions are pulled by a small constant electric field of $E \sim 10$ V/cm, and undergo collisions with a helium buffer gas at a pressure of $\sim$3 Torr. A pair of grids are located at the exit of the first drift tube, and before the entrance to the second drift-tube. By pulsing the voltage on the first grid one can allow only ions of a specific mobility to enter the second drift tube. By applying an activation voltage $V_{\rm act}$ between the two grids, the ions are collisionally activated which causes them to isomerize and possibly fragment. Subsequently the second drift tube is used to measure the resulting distribution of isomers. At the exit of the second drift tube the ions are pulsed into a time-of-flight mass spectrometer. The millisecond timescale of the mobility separation coupled to the microsecond timescale of the mass analysis allows these datasets to be collected in a nested fashion. Thus a typical measurement results in a two dimensional matrix, similar to that shown in Fig. 2(a), where the counts are imaged as a function of mass and drift time for the RPSB and no selection and activation voltages were applied. Such measurements are called 'source distribution'

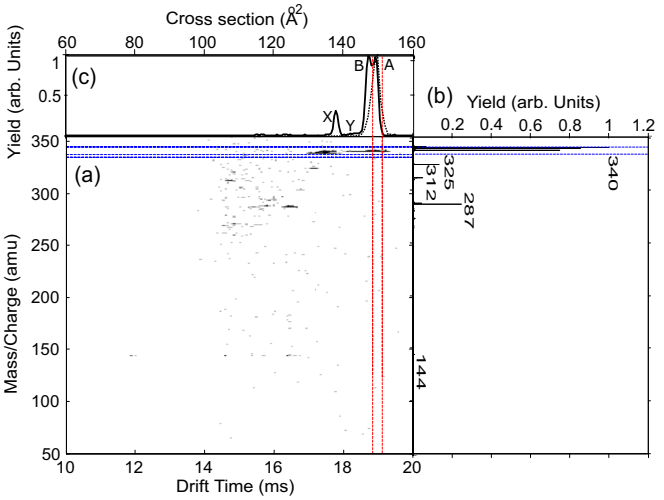

FIG. 2. Source distribution of RPSB. (a) The counts are imaged as a function of drift time and mass over charge. (b) Mass spectrum resulting from summing over the drift times. (c) IMS of the RPSB (solid), resulting from an integration over a narrow mass window around mass 340 m/z indicated by the blue dashed lines in (a). The dashed line represents the measured IMS after selection is applied to a narrow time window indicated by the red dashed lines, corresponding to peak A.

measurements as they reflect the distribution of molecular ions and their isomers produced in the ion source. Previous work has shown that under gentle source conditions this distribution is reflective of the isomer distribution present in the solution from which the sample is electrosprayed [17].

Summing over all drift times one arrives at a MS plot, shown in Fig. 2(b), which is similar to a MS measured in a typical mass spectrometer. In this case the MS shows a peak at mass 340 m/z corresponding to RPSB. Other, smaller, mass peaks appear which correspond to contaminations in the sample or to fragment ions created in the ion source. By integrating the counts over a narrow m/z range, indicated by the blue rectangle in Fig. 2(a), one arrives at a drift time distribution for that particular mass, as seen in Fig. 2(c) (solid), which is often converted into a cross section distribution.

When selection is applied to a narrow time window, and the activation voltage is set to low values, the drift-time distribution consists of a single peak, for example see the dashed line in Fig. 2(c) (dashed). When the activation voltage is high enough the ions begin to isomerize within the activation region and the second IMS distribution begins to vary. These measurements are called 'selection and activation' (SA) measurements. Figure 3 shows the results of an SA measurement, where selection is applied to the time window indicated by the two red lines in Fig. 2, corresponding to an IMS peak which we labeled as 'A', with $V_{\rm act} = 180$ V. Here, as a result of the activation, the IMS distribution of mass 340 is broad, indicating the formation of many isomers. In addition, due to fragmentation, peaks at lower masses also appear. From the drift-time one can extract the ions' mobility and their cross section for collisions with the helium buffer gas. The procedure for converting drift-times into cross section for SA measurements is detailed in Appendix A.

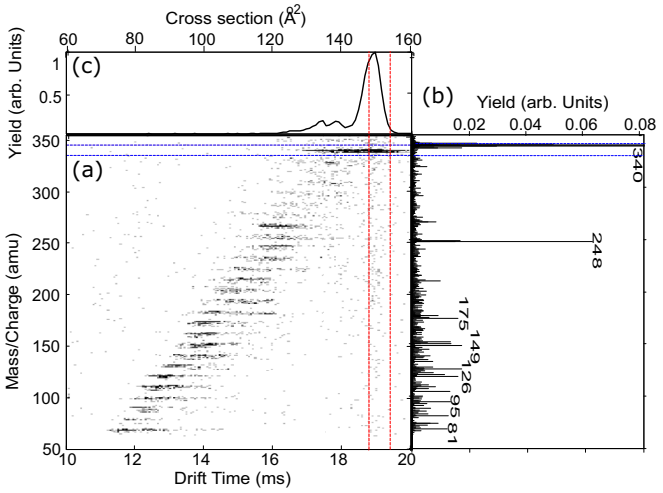

FIG. 3. Selection and activation measurement of the RPSB at $V_{act} = 180$ V with the selection applied to peak A. (a) The number of counts are plotted as a function of drift time and mass. (b) Mass spectrum resulting from summing over the drift times. (c) IMS of the RPSB resulting from an integration over a narrow mass window around mass 340 m/z.

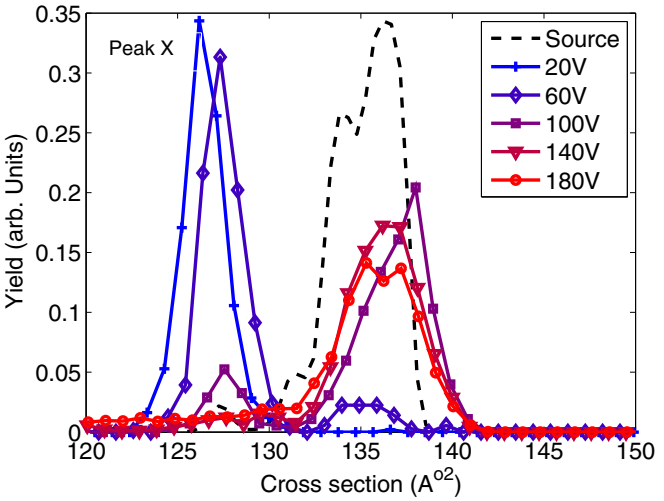

FIG. 5. Selection and activation measurements where selection is applied to peak X of the dimethylated RPSB, for various activation voltages V_{act}. The dashed black line corresponds to source distribution (when no selection and actibation is applied).

III. IMS-IMS-MS OF RPSB DERIVATIVES: RESULTS AND DISCUSSION

Figure 4(a) shows the source distribution of the RPSB and the three additional derivatives studied in this work. The RPSB has two prominent peaks, labeled A and B which correspond (according to cross section calculations) to the *all-trans* and *single-cis* isomers, respectively. For peak assignment we calculate the equilibrium geometries using density functional theory (DFT) based on the PBE0 exchange-correlation function [18] and the cc-pVTZ basis set [19] within the QCHEM code [20]. From the DFT equilibrium geometries the collision cross section for the different isomers were calculated using the MOBCAL program [21,22].

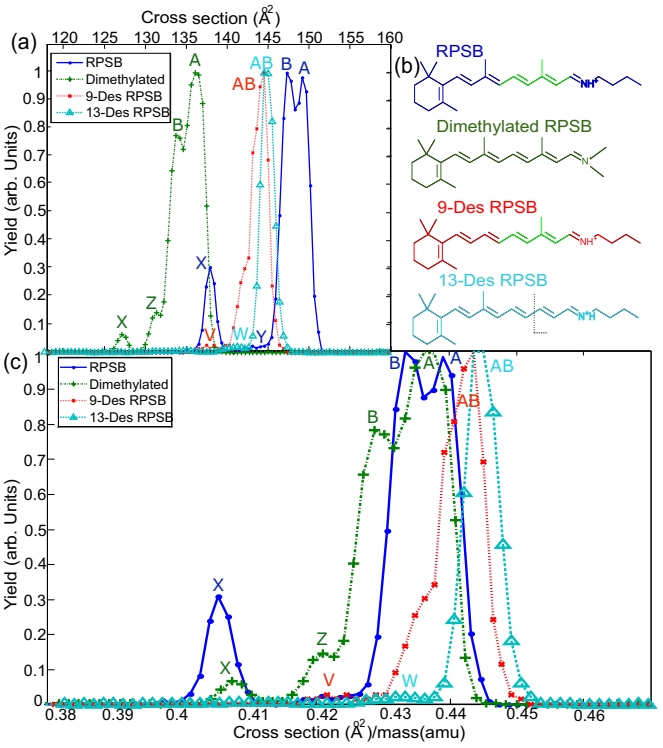

FIG. 4. (a) IMS of the retinal and the retinal derivatives. (b) The structure of the RPSB derivatives (c) The IMS of the retinal and the retinal derivatives where the x axis is the cross section divided by mass.

Two additional peaks of smaller abundance, labeled here as Y and X are also seen. These correspond, respectively, to *multiple-cis* and cyclized isomers, such as the ones illustrated in Fig. 1(d) and 1(e). The source distribution of the dimethylated RPSB is similar to that of the RPSB. It consists of four peaks but with a smaller cross section relative to the RPSB, since it is physically smaller. Because RPSB derivatives have roughly linear shapes, we expect their collision cross sections to be linearly correlated with their mass. Figure 4(c) plots each of the derivatives on a collision cross section scale that has been normalized by the mass of the derivative, which provides a near perfect overlay of each isomer population. The IMS of the 9-des RPSB and the 13-des derivatives are simpler than that of the RPSB, consisting of one dominant peak labeled here as AB for both derivatives, and a smaller peak. It is not yet clear to us if peak AB consists of only one of the two isomers seen for the regular RPSB, or that the two peaks are present but cannot be resolved. The IMS of both the 9-des and the 13-des also consists of a small peak corresponding to ions having a lower cross section, which we label as V and W, respectively.

Figures 5 and 6 show two examples of the SA measurements of the dimethylated RPSB. When selection is applied to peak X (Fig. 5) the isomer distribution does not change for $V_{act} < 60$ V. At 60 V peaks A and B begin to form and their population increases with V_{act}. When selection is applied to peak A (Fig. 6) the IMS distribution begins to broaden at $V_{act} = 130$ V, indicating the formation of peak B,

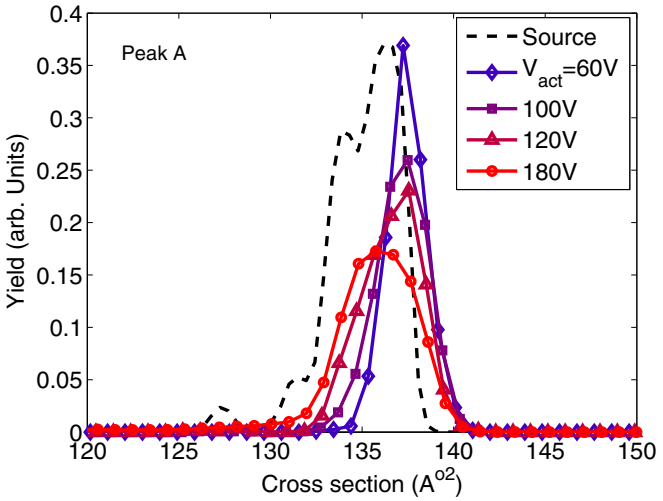

FIG. 6. Selection and activation measurements where selection is applied to peak A of the dimethylated RPSB, for various activation voltages V_{act}. The dashed black line corresponds to source distribution (when no selection and activation is applied).

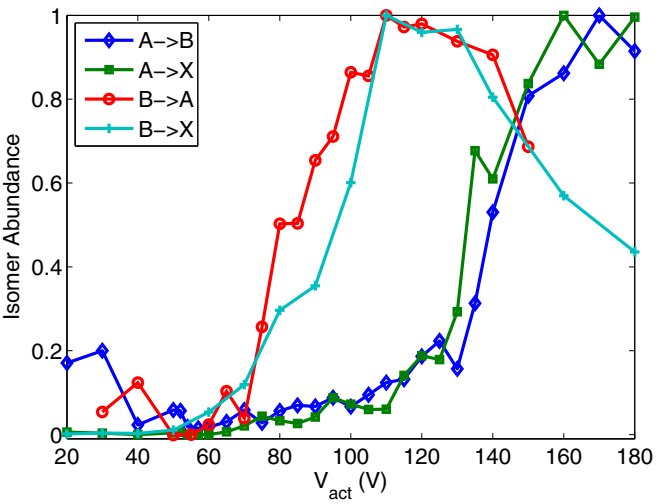

FIG. 7. Thresholds plots for several of the transitions of the dimethylated RPSB.

whereas peak X begins forming at a slightly lower voltage of $V_{\text{act}} = 120\,\text{V}$.

At high enough activation voltages the chromophores begin to fragment and the masses, and the mobilities of the fragments are measured. The 9-des derivative is found to have one prominent fragment at 234 m/z, which corresponds to toluene emission from the central part of the molecule, similar to that of the RPSB. However, 13-des shows one prominent fragment at 111 m/z, corresponding to the cleavage of the $C12$–$C13$ bond, a fragmentation process which does not involve cyclizations. The dimethylated RPSB does not have a single prominent fragmentation product, but rather has many fragmentation products, most of which correspond to bond cleavage along the polyene chain of the chromophore.

To determine the barrier energies for a transition between two structures, for example for the A $\rightarrow$ B transition, we use SA measurements with selection applied to peak A, and plot the count in the drift-time window corresponding to peak B. Examples of such threshold plots are shown in Fig. 7, for the case of the dimethylated RPSB. The threshold activation voltage is defined as a change in relative intensity of 1%. Similarly by plotting the number of fragment ions produced as a function of activation voltage, the threshold voltage for fragmentation is determined. Pierson *et al.* [23] showed that the activation voltages divided by the number of degrees of freedom of the molecule scales linearly with the barrier energies. Thus one can translate V_{act} into the barrier energies for fragmentation and isomerization. A full summary of the activation voltages for each transition of the four RPSB derivatives as well as the corresponding barrier energies is given in Appendix B. From the measured barrier energies for isomerization one can also deduce the relative ground state energies of the isomers in two different manners. Let E_1 and E_2 be the ground state energies of two isomers, let $E_{1\rightarrow 2}$ and $E_{2\rightarrow 1}$ be the transition energies and F_1 and F_2 be the fragmentation energies of each of the isomers. The energy difference between the two isomers $\Delta E = E_2 - E_1$ is given by $\Delta E = F_2 - F_1$, as well as by $\Delta E = E_{2\rightarrow 1} - E_{1\rightarrow 2}$. In all the cases studied here there is a consistency in that the ΔE determined from the barrier energies agrees with that determined from the barriers for fragmentation.

Figure 8 is a schematic illustration of the potential energy landscape of the four RPSB derivatives based on the relative energies and barrier energies for isomerizations that are detailed in Appendix B. In previous work, the energy barrier for isomerization of the RPSB was extensively discussed [15]. For the case of the dimethylated RPSB the barrier energies for isomerization and fragmentation are higher than for the RPSB. For example, the biologically important *single-cis* to *all-trans* isomerization is a factor of 1.3 higher. One possible explanation involves the mobile proton model [24]. Within peptides it is often found that a mobile proton facilitates isomerization, weakens bonds, and causes fragmentation to occur in specific places. Thus the absence of the proton attached to the nitrogen in the dimethylated derivative may explain the higher barriers for isomerization. Another possible explanation for the increase in barrier energies has to do with

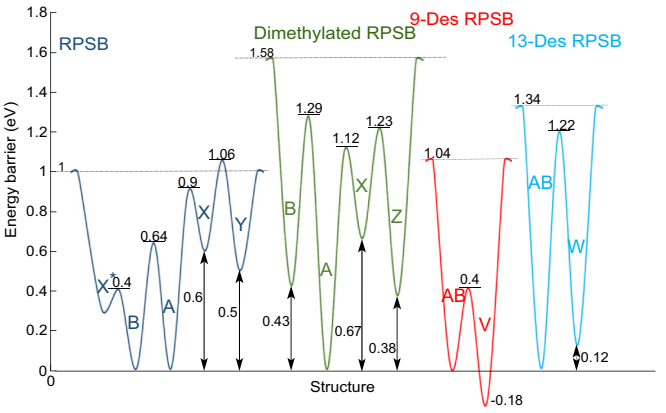

FIG. 8. Schematic illustration of the ground-state energies and the energy barrier for isomerization of the RPSB and the RPSB derivatives measured here.

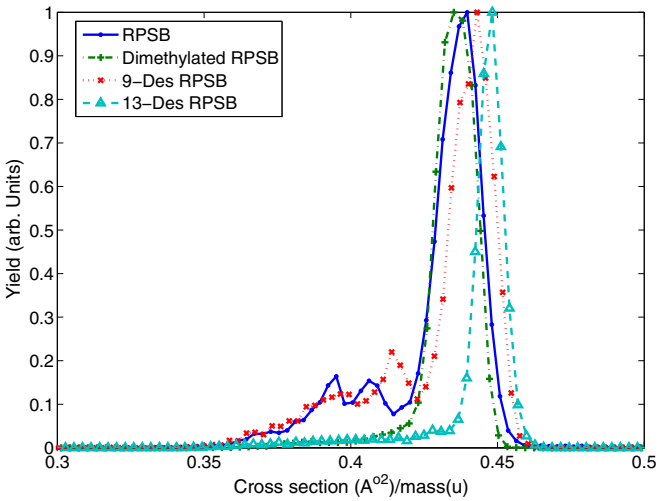

FIG. 9. Quasi-equilibrium distribution of the RPSB and the RPSB derivatives where at the x axis the cross section is dividing by the mass of the molecule, measured at $V_{\text{act}} = 180\,\text{V}$.

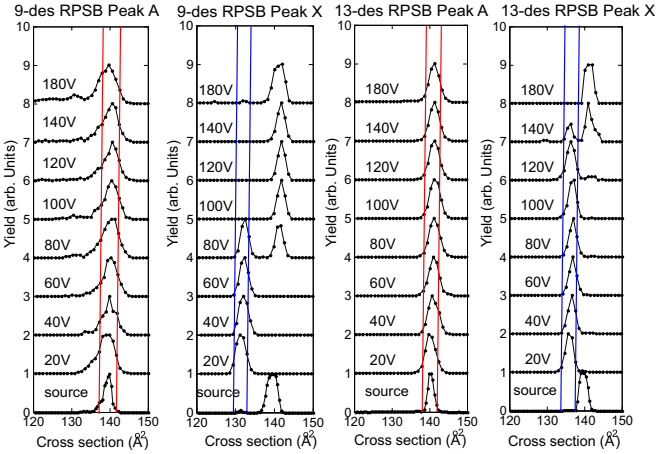

FIG. 10. IMS-IMS distribution as a function of activation voltage when selection applied on peak A and X of the 9-des and 13-des RPSB derivatives.

the fact that in the dimethylated derivative the positive charge is more localized on the nitrogen atom. Indeed, one would expect that the more localized the charge, the higher the barrier energies for isomerization.

For the 9-des and 13-des derivatives one would expect a smaller increase in the barrier energies as the charge is a little more localized than for the RPSB. Differences in the excited state dynamics have been observed for the 9-des and 13-des derivatives, both in Rhodopsin proteins [25–27] and in gas phase calculations [28]. Here, we observe marked differences in the ground state dynamics between the two derivatives in that the barrier energy for cyclization is a factor of 3 higher for the 13-des relative to the 9-des. Furthermore, while the 9-des fragments through cyclization the 13-des fragments through the cleavage of the $C12$–$C13$ bond. We can conclude that the methyl on position $C13$ plays a pivotal role on ground state dynamics. Interestingly, the 9-des is the only derivative we have seen so far in which the cyclized isomer has lower energy than the AB peak.

When the activation energy is much greater than the barrier energies the structures reach a quasi-equilibrium (QE) distribution of states [29]. This gas-phase equilibrium distribution appears to be the same regardless of which structure was selected and activated. Figure 9 shows the collision cross section distributions (normalized by mass) of the QE distributions for each of the four RPSB derivatives studied here. We find that there is a correlation between the QE distributions and the gas phase fragmentation patterns of the chromophores. The RPSB and the 9-des, have similar QE distributions which are different than those of the dimethylated and 13-des derivatives in that they contain a more prominent contribution from compact isomers with reduced cross section of $\approx 0.4\frac{\text{Å}}{m/z}$. This fits well with the fragmentation mechanisms, as both RPSB and 9-des RPSB fragment through toluene emission, a process which involves cyclization and the formation of compact intermediate structures. The 13-des and dimethylated derivatives do not.

IV. CONCLUSIONS

These measurements allow us to quantify the relation between charge delocalization and chromophore rigidity. Specifically, we find that localizing the positive charge on the nitrogen atom by an additional methyl group increases the barrier energies for isomerization by a factor of 1.3. Additionally the methyl on the $C13$ position has a more pivotal role on ground state dynamics as its absence results in a strong increase in the barrier energy for cyclization and in a different fragmentation pattern. Since even slight changes in the RPSB structure significantly effect the chromophores energetic landscape, it may well be that the RPSB has optimal properties for a photoswitch explaining its use in every known form of animal vision.

ACKNOWLEDGMENTS

We are grateful to Igor Schapiro (HUJI), Anastasia V. Bochenkova (Moscow State University), and Steen Brøndsted Nielsen (Aarhus University) for their advice and insights in this project. J.D. acknowledges the support from NSWC Crane Division Naval Innovative Science and Engineering Program. This research was supported by GIF Research Grant No. I-2370-303.7/2014, and by the Israel Science Foundation.

APPENDIX A: CROSS SECTION DETERMINATION IN SELECTION AND ACTIVATION MEASUREMENTS

In order to interpret the results of selection and activation measurements, such as those shown in Figs. 5 and 6 and in greater detail in Fig. 10, one has to translate the experimentally measured drift time into cross section, and properly account for the change in drift time due to the higher electric field within the activation region. This procedure is detailed below.

Ion mobility, K, is defined as the ratio between the drift velocity, v_d, and the applied electric field, $E = \frac{V}{L}$ (where L is the length of the drift tube, and V is the voltage drop):

$$K = v_d E = \frac{L}{t_D E} = \frac{L^2}{t_D V}, \tag{A1}$$

TABLE I. Threshold activation voltages and barrier energies for isomerization and fragmentation of the RPSB.

Transition	$V_{\mathrm{act}}(V)$	$E_b(V)$
$A->X$	100 ± 10	0.9 ± 0.12
$B->X$	40 ± 10	0.39 ± 0.12
$Y->A$	60 ± 10	0.56 ± 0.12
$Y->B$	60 ± 10	0.56 ± 0.12
$Y->X$	50 ± 10	0.47 ± 0.12
$X->A$	50 ± 10	0.47 ± 0.12
$X->B$	50 ± 10	0.47 ± 0.12
$A->B$	70 ± 10	0.64 ± 0.12
$B->A$	70 ± 10	0.64 ± 0.12
$A->$ frag	110 ± 10	1 ± 0.12
$B->$ frag	110 ± 10	1 ± 0.12
$Y->$ frag	50 ± 10	0.5 ± 0.12
$X->$ frag	40 ± 10	0.4 ± 0.12

$E:K$ determination where t_D is the time it takes the ions to traverse the drift tube. The mobility is inversely linear with the collisional cross section:

$$\Omega=\frac{\sqrt{18\pi}}{16}\frac{ze}{\sqrt{k_BT\mu}}\frac{1}{K}\left(\frac{760}{P}\right)\left(\frac{T}{273.2}\right)\frac{1}{N}. \tag{A2}$$

Here ze is the ion's charge, k_B is the Bolzmann constant, L is the length of the drift tube, μ is the reduced mass of the ions and buffer gas molecules, T is the temperature, and N is the neutral number density at standard temperature and pressure.

In selection and activation measurements the motion is composed of three subsequent step:

(i) Passage through a drift tube of length L_1, under the influence of an electric field E_1.

(ii) Passage through the activation region of length L_A, where an activation voltage V_A is applied.

TABLE II. Threshold activation voltages and barrier energies for isomerization and fragmentation of the dimethylated RPSB.

Transition	$V_{\mathrm{act}}(V)$	$E_b(V)$
$A->B$	130 ± 5	1.29 ± 0.08
$A->Y$	125 ± 5	1.24 ± 0.08
$A->X$	115 ± 5	1.14 ± 0.08
$B->A$	85 ± 5	0.85 ± 0.08
$B->Y$	115 ± 5	1.14 ± 0.08
$B->X$	60 ± 5	0.61 ± 0.08
$X->A$	50 ± 10	0.52 ± 0.13
$X->B$	40 ± 10	0.42 ± 0.13
$X->Y$	50 ± 5	0.52 ± 0.08
$Y->A$	100 ± 10	0.9 ± 0.13
$Y->B$	120 ± 10	1.19 ± 0.13
$Y->X$	80 ± 10	0.8 ± 0.13
$A->$ frag	160 ± 10	1.58 ± 0.13
$B->$ frag	115 ± 5	1.14 ± 0.08
$X->$ frag	90 ± 10	0.9 ± 0.13
$Y->$ frag	120 ± 10	1.19 ± 0.13

TABLE III. Threshold activation voltages and barrier energies for isomerization and fragmentation of the 9-des RPSB.

Transition	$V_{\mathrm{act}}(V)$	$E_b(V)$
$A->X$	40 ± 10	0.4 ± 0.13
$X->A$	60 ± 5	0.58 ± 0.08
$A->$ frag	110 ± 10	1.04 ± 0.13
$X->$ frag	130 ± 5	1.22 ± 0.08

(iii) Passage through the second drift tube of length L_1, under the influence of an electric field E_1.

In these measurements the ions have a mobility K_1 before the activation region, and possibly a different mobility K_2 after the activation region. We use here a simplified assumption that the mobility changes exactly at the exit of the activation region (although in practice it may change in any place inside the activation region). Therefore the total drift time will be given according to

$$t_{\mathrm{tot}}=\frac{1}{K_1}\left(\frac{L_1^2}{V_1}+\frac{L_A^2}{V_A}\right)+\frac{1}{K_2}\left(\frac{L_1^2}{V_1}\right). \tag{A3}$$

Using measurements of selection without activation we determine the initial mobility of the ions K_1, which we then use to determine K_2 according to

$$\frac{1}{K_2}=\frac{V_1}{L_1^2}\left[t_{\mathrm{tot}}-\frac{1}{K_1}\left(\frac{L_1^2}{V_1}+\frac{L_A^2}{V_A}\right)\right]. \tag{A4}$$

APPENDIX B: BARRIER ENERGIES DETERMINED IN THIS WORK

Determination of barrier energies for isomerization and fragmentation on measuring the threshold activation voltages, and converting them to barrier energies based on the semi-quantitative method introduced by Pierson *et al.* [1]. Notably, the present work was conducted on the same apparatus, with the same conditions, such that the calibration of activation voltage to barrier height could be used [23]. The results are summarized in Tables I–IV.

TABLE IV. Threshold activation voltages and barrier energies for isomerization and fragmentation of the 13-des RPSB.

Transition	$V_{\mathrm{act}}(V)$	$E_b(V)$
$A->X$	130 ± 5	1.22 ± 0.08
$X->A$	120 ± 10	1.13 ± 0.13
$A->$ frag	150 ± 5	1.34 ± 0.08
$X->$ frag	130 ± 10	1.22 ± 0.13

[1] N. A. Pierson and D. E. Clemmer, Int. J. Mass Spectrom. **377**, 646 (2015).
[2] R. R. Birge, Biochim. Biophys. Acta **1016**, 293 (1990).
[3] R. W. Schoenlein, L. A. Peteanu, R. A. Mathies, and C. V. Shank, Science **254**, 412 (1991).
[4] R. Govindjee, S. Balashov, and T. Ebrey, Biophys. J. **58**, 597 (1990).
[5] J. Herbst, Science **297**, 822 (2002).
[6] R. B. Barlow, R. R. Birge, E. Kaplan, and J. R. Tallent, Nature **366**, 64 (1993).
[7] S. Gozem, I. Schapiro, N. Ferre, and M. Olivucci, Science **337**, 1225 (2012).
[8] *Photophysics of Ionic Biochromophores*, 1st ed., edited by S. B. Nielsen and J. A. Wyer, Physical Chemistry in Action (Springer, New York, 2013).
[9] J. Rajput, D. B. Rahbek, L. H. Andersen, A. Hirshfeld, M. Sheves, P. Altoe, G. Orlandi, and M. Garavelli, Angew. Chem., Int. Ed. **49**, 1790 (2010).
[10] Y. Toker, D. B. Rahbek, H. V. Kiefer, J. Rajput, R. Antoine, P. Dugourd, S. B. Nielsen, A. V. Bochenkova, and L. H. Andersen, Phys. Chem. Chem. Phys. **15**, 19566 (2013).
[11] N. J. A. Coughlan, B. D. Adamson, K. J. Catani, U. Wille, and E. J. Bieske, J. Phys. Chem. Lett. **5**, 3195 (2014).
[12] L. Musbat, M. Nihamkin, S. Ytzhak, A. Hirshfeld, N. Friedman, J. M. Dilger, M. Sheves, and Y. Toker, J. Phys. Chem. A **120**, 2547 (2016).
[13] N. J. A. Coughlan, K. J. Catani, B. D. Adamson, U. Wille, and E. J. Bieske, J. Chem. Phys. **140**, 164307 (2014).
[14] N. J. A. Coughlan, B. D. Adamson, L. Gamon, K. Catani, and E. J. Bieske, Phys. Chem. Chem. Phys. **17**, 22623 (2015).
[15] J. Dilger, L. Musbat, M. Sheves, A. V. Bochenkova, D. E. Clemmer, and Y. Toker, Angew. Chem. **127**, 4830 (2015).
[16] S. L. Koeniger, S. I. Merenbloom, S. J. Valentine, M. F. Jarrold, H. R. Udseth, R. D. Smith, and D. E. Clemmer, Anal. Chem. **78**, 4161 (2006).
[17] N. A. Pierson, L. Chen, S. J. Valentine, D. H. Russell, and D. E. Clemmer, J. Am. Chem. Soc. **133**, 13810 (2011).
[18] Y. T. Shao, Phys. Chem. Chem. Phys. **8**, 3172 (2006).
[19] T. H. Dunning, J. Chem. Phys. **90**, 1007 (1989).
[20] C. Adamo and V. Barone, J. Chem. Phys. **110**, 6158 (1999).
[21] M. F. Mesleh, J. M. Hunter, A. A. Shvartsburg, G. C. Schatz, and M. F. Jarrold, J. Phys. Chem. **100**, 16082 (1996).
[22] A. A. Shvartsburg and M. F. Jarrold, Chem. Phys. Lett. **261**, 86 (1996).
[23] N. A. Pierson, L. Chen, D. H. Russell, and D. E. Clemmer, J. Am. Chem. Soc. **135**, 3186 (2013).
[24] V. H. Wysocki, G. Tsaprailis, L. L. Smith, and L. A. Breci, J. Mass Spectrom. **35**, 1399 (2000).
[25] Y. Shichida, A. Kropf, and T. Yoshizawa, Biochemistry **20**, 1962 (1981).
[26] G. G. Kochendoerfer, P. J. E. Verdegem, I. van der Hoef, J. Lugtenburg, and R. A. Mathies, Biochemistry **35**, 16230 (1996).
[27] Q. Wang, G. G. Kochendoerfer, R. W. Schoenlein, P. J. E. Verdegem, J. Lugtenburg, R. A. Mathies, and C. V. Shank, J. Phys. Chem. **100**, 17388 (1996).
[28] I. Schapiro, J. Phys. Chem. A **120**, 3353 (2016).
[29] N. A. Pierson, S. J. Valentine, and D. E. Clemmer, J. Phys. Chem. B **114**, 7777 (2010).